Technical Report

Muon Tomography of Underground Fracture Zones

Gábor Nyitrai,[1,2] László Balázs,[1] Gergely Surányi,[1] Constantin D. Athanassas,[3] and Dezső Varga[1]

[1]*HUN-REN Wigner Research Centre for Physics, Budapest 1121, Hungary*

[2]*Budapest University of Technology and Economics, 1111 Budapest, Hungary*

[3]*National Technical University of Athens, 15780 Athens, Greece*

Corresponding author: Gábor Nyitrai
Email address: nyitrai.gabor@wigner.hu

Abstract

A high resolution muography survey has been performed in the Királylaki tunnel in Budapest (Hungary) to search for unknown cavities. Preliminary radiographic measurements suggested large density anomalies above the tunnels in a 20–60 m thick cherty dolomite rock (2.5–2.7 g/cm^3). A Bayesian inversion method has been adapted to overcome the underdetermination originating from the limited-angle tomographic nature of muography. The angular resolution of the gaseous muon detectors enabled a spatial voxel resolution of 1-2 meters, and the 3D distribution of karstic fracture zones has been obtained. Multiple 5–10 m long core drills validated the existence of low-density regions. The core samples showed convincing agreement with the inversion, containing fractured rock (altered dolomite powder, below 1.8 g/cm^3). This work confirms the potential of mapping underground fracture zones using muography, which has potential applications in tunnel construction and maintenance, as well as for landslide studies, depending upon feasible boundary conditions.

Keywords: muography, inversion, numerical solution, fracture zones
DOI: 10.31526/JAIS.2024.493

1. INTRODUCTION: WHY FRACTURE ZONE IMAGING IS INTERESTING

Underground low-density regions may result from fracture zones in the crust of the Earth, created by hydraulic or tectonic processes. Collapse of fracture zones can be highly dangerous for society in multiple circumstances. In Figure 1, an example of a landslide affecting the city of Santa Tecla (El Salvador) is depicted on the left, while on the right, a geological chart illustrates the intersection of a linear infrastructure with a faulted zone. Interestingly, for the construction of any underground facility, the work is not easier through light-structured rocks, but actually makes it more difficult, since the facility must be made robust against the collapse of the surrounding rock.

Finding fracture zones with conventional geophysical imaging methods (e.g., gravimetry, seismic, or electric resistivity survey) can be a difficult task since the resolution of these methods is usually much lesser than that of muography and these zones are usually thin layers (a few meters) in the contact boundary of different rock bodies. Therefore, muography can be a powerful tool to image fracture zones [2, 3, 4, 5, 6] or lahars [7], if geometric conditions are met (e.g., the detector can be positioned below the object), and supply data for a landslide or tunnel collapse risk assessment.

2. DENSITY ANOMALIES IMAGED FROM THE KIRÁLYLAKI TUNNELS

Hungary, and also Budapest, is blessed with wonderful natural treasures, as there are many beautiful caves that can be visited within the city limits. Therefore, speleology is flourishing, and finding new caves is a hot topic for potential tourist attractions. We are conducting multiple cave research projects in Hungary, and this was the original reason for the beginning of a muography survey in the Királylaki ("King lair") tunnels. These tunnels were constructed as a pilot project for the underground gas reservoir in the 1960s, but the project was terminated. However, the tunnels crossed a natural cave which was found and explored in the last decades. Therefore, these tunnels provided an ideal and promising location for cavity search with muography.

We collected high-resolution muograph data in multiple locations with a 40 cm $\times$ 40 cm CCC (Close Cathode Chamber) detector [8], $\sim$1-month data per location. As it is shown in Figure 2, several complex density anomalies were found above the tunnels. Spatial localization started with triangulation since clearly distinguishable low-density objects were found. However, since the feasibility of an exploratory core drill for us is limited to 10 meters, the practical question arose: which is the closest point of the anomalies and where to drill? To determine the spatial density distribution, we provided a solution by applying a Maximum Likelihood-based least squares tomography method with Bayes criterion [12].

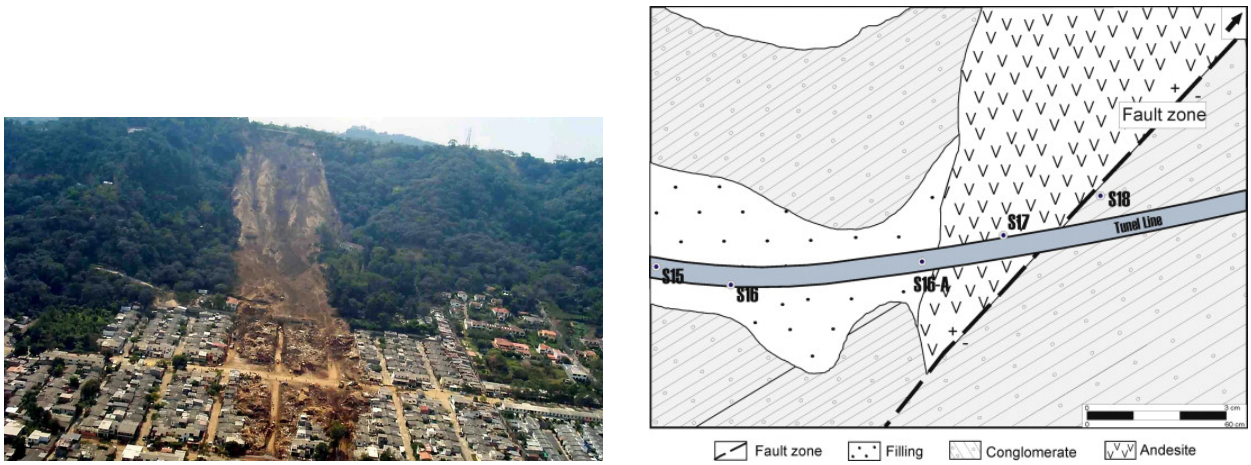

FIGURE 1: Examples of fracture zone hazards. *Left*: Landslide (image: NASA). *Right*: Tunnelling through fault zone [1].

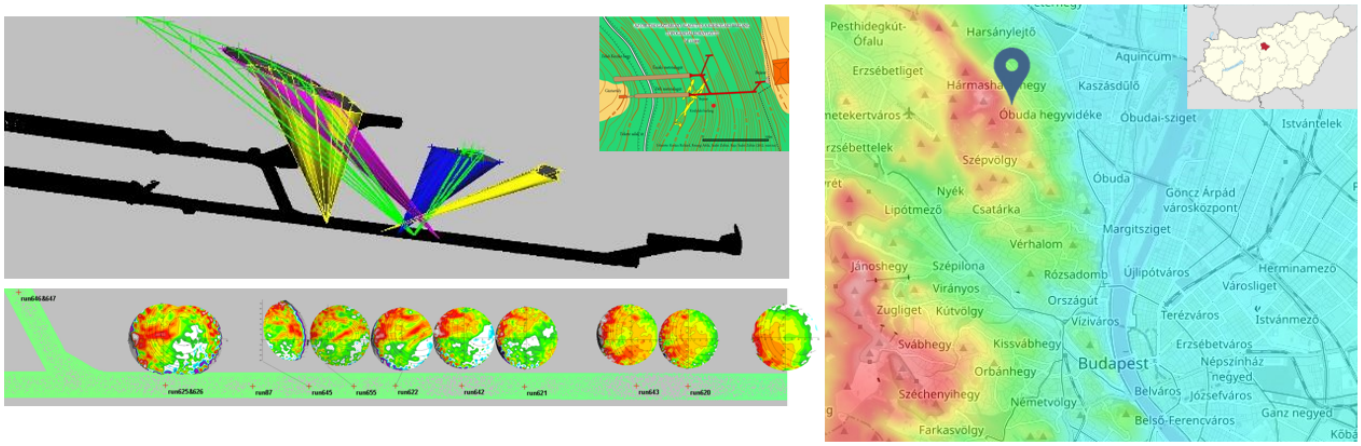

FIGURE 2: Several density anomalies were found above the Királylaki tunnel, Budapest. On the top left panel, the imaging cones of these anomalies are shown from different detector positions along the tunnel, as well as density anomaly maps below (red-green-white is where the density is much lower, less low, and equal to the bedrock, respectively). The right panel shows the location of the tunnel in Budapest, Hungary.

3. INVERSION ALGORITHM WITH BAYESIAN CONSTRAINTS

Spatial reconstruction of density distribution from density-length projections is inherently a tomographic "inverse" problem, that is, a process of calculating from a set of integrated observations the causal factors (density distribution) that produced them. The density lengths in the given measurement directions were obtained by converting muon fluxes using Guan's parametrization [9], and the results were cross-checked with Reyna's method [10]. The minimum energy required for the conversion is obtained from Lesparre's parametrization [11]. The base equation of the (linearized and discretized) inverse problem is

$$\gamma = \mathbf{F}\rho, \tag{1}$$

where γ is the combined vector of directional density lengths (transformed from muon flux measurements), ρ is the combined vector of the searched densities in all the voxels of the imaged volume, and $\mathbf{F}$ is the matrix of mapping from the voxels to the directional measure bins (integral projection along the cone of solid angle). To put it simply, the inversion problem of muography is to find ρ such that the $\mathbf{F}$ matrix is not invertible.

The issues with the bare application of any tomographic inversion algorithm are the imperfect mapping between the voxel grid and measure bins, the underdetermination (more voxels than measurements) and limited detector positioning (limited-angle tomography) which inherently causes artifacts in the results, the inhomogeneous and low statistics (relative to, e.g., computed tomography scans), systematic uncertainties of muography, etc. To handle the issues, we adopted an inversion algorithm based on the Bayes criterion, Maximum Likelihood, linearization (inversion input is density length and not muon flux), and 2D simplification: reconstruction in multiple planes intersecting the measurement line [12]. The parameter bias and artifacts can be also controlled by calculating the measurement uncertainty weights in the voxel base ($\mathbf{W}_\gamma$).

Functional to be minimized follows from the weighted least squares of $(\boldsymbol{\gamma} - \mathbf{F}\boldsymbol{\rho})$ and the Bayes parameters $(\boldsymbol{\rho} - \boldsymbol{\rho}^{(0)})$ to be fitted:

$$Q^{(0)} = Q_{\gamma}^{(0)} + Q_{\rho}^{(0)} = (\boldsymbol{\gamma} - \mathbf{F}\boldsymbol{\rho})^T \mathbf{W}_{\gamma} (\boldsymbol{\gamma} - \mathbf{F}\boldsymbol{\rho}) + \left(\boldsymbol{\rho} - \boldsymbol{\rho}^{(0)}\right)^T \mathbf{W}_{\rho}^{(0)} \left(\boldsymbol{\rho} - \boldsymbol{\rho}^{(0)}\right), \tag{2}$$

and from that, the estimation of the density distribution can be derived as follows [12]:

$$\boldsymbol{\rho}^{(1)} = \left(\mathbf{R} + \mathbf{W}_{\rho}^{(0)}\right)^{-1} \left(\mathbf{F}^T \mathbf{W}_{\gamma} \boldsymbol{\gamma}_m + \mathbf{W}_{\rho}^{(0)} \boldsymbol{\rho}^{(0)}\right), \tag{3}$$

where $\mathbf{R} = \mathbf{F}^T \mathbf{W}_{\varrho} \mathbf{F}$ is the Fischer matrix.

4. TOMOGRAPHY RESULTS

The Bayesian inversion applied to the measurements resulted in tilted layers of density anomalies (Figure 3 (right)). In the left panel of the figure, the perpendicular cross-section of the applied 2D inversion slicing scheme [12] is shown. The right panel shows the density distribution results in one of the slices. The results indicate that the anomalies are located along planes like fracture zones, and the closest points of the anomalies are easy to read from the figure.

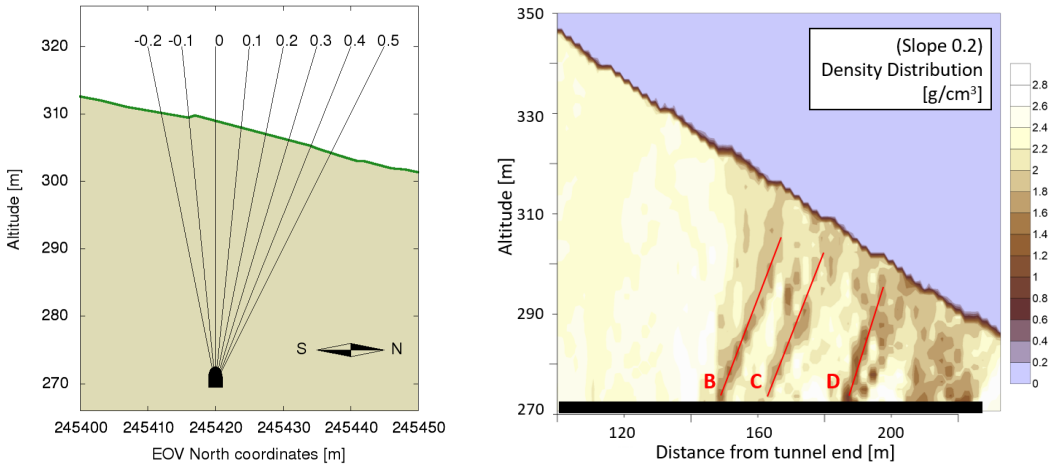

FIGURE 3: *Left*: Applied 2D slicing scheme, perpendicular to the straight tunnel. Each slice (marked from -0.2 to 0.5, the zenith tangent slope of a given slice) represents a plane in which 2D inversions were calculated. *Right*: Density reconstruction results in one of the slices (slope 0.2) parallel to the tunnel. The results show multiple fracture zones, named B, C, and D.

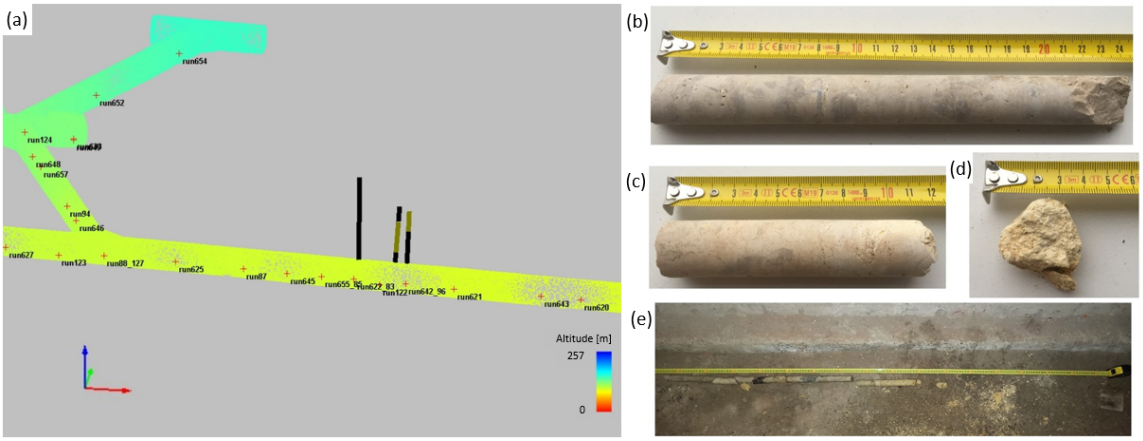

FIGURE 4: (a) The digital elevation map of the tunnel with the indication of the three-core drilling. Dots are showing detector positions (those in the side passages were not used in this evaluation). Core drilling samples from the base rock (b, c), the anomalous region (d), and the last two meters of one drilling along its entire length (e).

Core drillings were done in three locations (5–10 m lengths) [12] into the anomalies for validation (Figure 4 (left)). The density measurement of the core samples showed convincing agreement with the inversion results, which did not contain cavities but a low-density fractured rock (altered dolomite powder with $<1.8\,\mathrm{g/cm^3}$ density) in the base rock ($\sim 2.6\,\mathrm{g/cm^3}$).

Figure 4 right panel shows the actual core samples from different relevant rock zones: (b) intact cherty dolomite (2.6–2.7 g/cm^3), (c) slightly altered dolomite close to the walls of the fissures (2.4–2.5 g/cm^3), (d) altered dolomite powder (less than 1.8 g/cm^3), and (e) the full extent of the last 2 m drill core from one of the drill hole. Dolomite powder only partially recovered (most of the dolomite powder has been washed away by the water of the diamond core driller, making it difficult to even continue the drilling operation).

5. FURTHER PERSPECTIVES

5.1. Királylaki Landslide Hazard Assessment

A Hungarian geological book from 1929 [13] already reported fracture zones and landslides in the nearby region of Királylaki (east side of Tábor Hill) which pose hazards to human infrastructure (Figure 5 (left)). A classified technical drawing for the Királylaki gas reservoir tunnels from the 1960s also contains fracture zones (Figure 5 (right) A and B), which made constructions difficult. The "B" fracture is exactly in the same place as we found in our results shown in Figure 3. In the future, we will continue the measurements further inside the tunnels to image also fracture "A" and collect all relevant geological information and geophysical measurements to assess landslide risk, since several new housing estates were established very close to the entrance of the tunnel in the last decades.

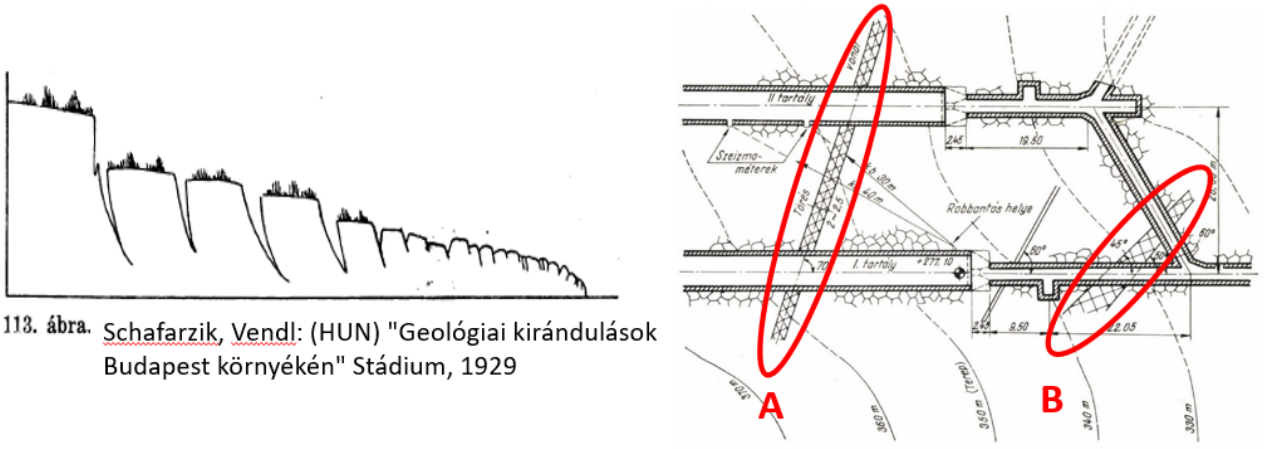

FIGURE 5: *Left*: Landslide and fracture formation in the surrounding region of Királylaki described in a geological book from 1929. *Right*: The classified technical drawing for the Királylaki gas reservoir tunnels from the 1960s contains one of the found fracture zones (B).

5.2. Santorini Fracture Zone Search Proposal

The city of Fira, the capital of the Greek island of Santorini, is famous for its unique architecture on top of a 400-meter-high caldera cliff. However, geologists are concerned about the existing Fira fault and unknown secondary fault zones under the city [14]. A muography survey from the Old Harbor; however, offers ideal imaging possibilities to determine the structure of the caldera, which is highly prone to landslides [15]. The feasibility conditions for a muographic survey have been examined, shown in Figure 6, with preliminary muon flux (top-right panel), calculated from the expected rock lengths (bottom-right panel).

CONFLICTS OF INTEREST

The authors declare that there are no conflicts of interest regarding the publication of this paper.

ACKNOWLEDGMENTS

This work has been supported by the Joint Usage Research Project (JURP) of the University of Tokyo, ERI, under project ID 2023-H-03, the "INTENSE" H2020 MSCA RISE project under GA No. 822185, the "Mine.io" HEU project under GA No. 101091885, the Hungarian NKFIH research grant under ID OTKA-FK-135349 and TKP2021-NKTA-10, the János Bolyai Scholarship of the HAS and the ELKH-KT-SA-88/2021 grant. The construction and testing of the detector were completed within the Vesztergombi Laboratory for High Energy Physics (VLAB) at Wigner RCP.

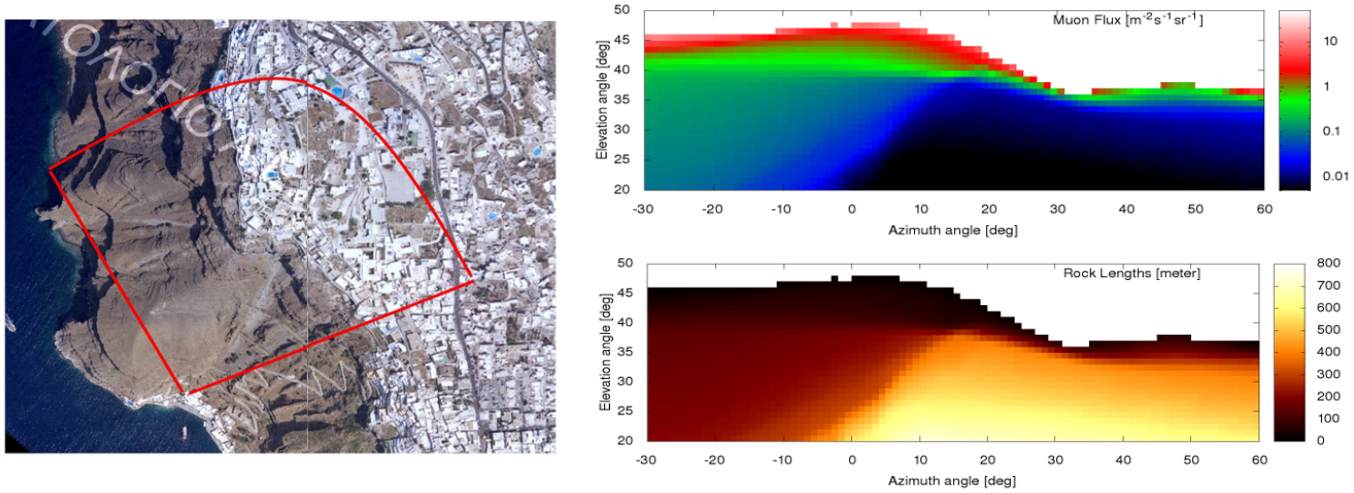

FIGURE 6: Proposed muography survey on the island of Santorini. *Left*: Satellite image about the possible imaged region (marked in red). *Right*: Expected rock lengths with Standard Rock density (bottom) and the associated muon flux (top).

References

[1] M. Kun and T. Onargan, Tunn. Undergr. Space Technol. **33**, 34–45, (2013). doi: 10.1016/j.tust.2012.06.016
[2] H. K. M. Tanaka et al., Geosci. Instrum. Method. Data Syst. **9**, 357–364, (2020). doi: 10.5194/gi-9-357-2020
[3] D. Borselli et al., Sci Rep **12**, 22329, (2022). 10.1038/s41598-022-26393-7
[4] S. Miyamoto et al., Ann. Geophys. **60**, S0110, (2017). doi: 10.4401/ag-7385
[5] S. Andringa et al., Muon Tomography in Lousal Mine (LouMu), https://pages.lip.pt/loumu/en/loumu/ (Accessed 25 September 2023)
[6] G. Baccani et al., J. Appl. Geophys. **191**, 104376 (2021). doi: 10.1016/j.jappgeo.2021.104376
[7] Oláh, L., Tanaka, H. K. M., Hamar, G., Sci. Rep. **11**, 17729 (2021). doi: 10.1038/s41598-021-96947-8
[8] D. Varga et al., Nucl. Instrum. Methods Phys. Res. A **698**, 11–18, (2013). doi: 0.1016/j.nima.2012.09.025
[9] M. Guan et al., arXiv:1509.06176 [hep-ex], (2015). doi: 10.48550/arXiv.1509.06176
[10] D. Reyna, arXiv:hep-ph/0604145, (2006). doi: 10.48550/arXiv.hep-ph/0604145
[11] N. Lesparre et al., Geophys. J. Int. **183**, 1348–1361, (2010). doi: 10.1111/j.1365-246X.2010.04790.x
[12] L. Balázs et al., Geophys. J. Int. **236**, 700–710 (2024). doi: 10.1093/gji/ggad428
[13] F. Schafarzik and A. Vendl, (Hungarian) Geológiai kirándulások Budapest környékén. Stádium, (1929).
[14] V. Antoniou et al., Proceedings of the 3rd International Conference on Geographical Information Systems Theory, Applications and Management—GISTAM (2017). doi: 10.5220/0006385801310141
[15] C. D. Athanassas, Med. Geosc. Rev. 2, 233–246 (2020). doi: 10.1007/s42990-020-00020-x